Kink grain boundaries in a block copolymer lamellar phase

M. W. Matsen
Polymer Science Centre, University of Reading, Whiteknights, Reading RG6 6AF, United Kingdom

(Received 28 April 1997; accepted 13 August 1997)

We introduce a method for examining the boundaries between periodic block copolymer morphologies using self-consistent field theory (SCFT). The technique is illustrated on kink grain boundaries in the AB diblock copolymer lamellar phase. In agreement with experiment, the A and B domains evolve from a simple ''chevron'' shape to a complex ''omega'' shape as the kink angle θ increases beyond about 90°. The transformation begins with the formation of an ''intermediate'' shape where protrusions develop symmetrically from the A and B domains at the center of the grain boundary. Following that, a continuous symmetry-breaking transition occurs forming the omega boundary where protrusions extend only from either the A or B domains. At low angles, in the chevron region, the grain boundary tension Γ_K obeys the scaling relation $\Gamma_K \sim \theta^3$, and at high angles, in the omega region, the tension peaks and then decreases with increasing angle. Raising the segregation in the melt causes a monotonic increase in the grain boundary tension; at strong segregations, the tension should scale as $\Gamma_K \sim \chi^{1/2}$, where χ is the Flory-Huggins interaction parameter. Both compositional and conformational asymmetries in the diblock molecule produce a decrease in Γ_K. © *1997 American Institute of Physics.* [S0021-9606(97)51243-8]

I. INTRODUCTION

The study of block copolymer melts has progressed to the stage where the equilibrium bulk phase behavior is well understood.[1,2] Researchers are now beginning to tackle problems involving kinetics and nonequilibrium behavior.[3] In equilibrium, block copolymer morphologies are well-ordered infinitely periodic structures. Although, there are presumably conditions, particularly at high temperatures, where fluctuations create a variety of small transient defects, their numbers are expected to be small. However, melts are typically not in equilibrium and the microstructural order is limited to finite-size regions separated by grain boundaries. Furthermore, the individual regions, or rather grains, will generally be populated by numerous local defects. This nonequilibrium structure is dependent on the sample preparation,[4] and should anneal out in time. High-energy defects are expected to anneal out quickly, but low-energy ones can persist for extremely long times.[4] Consequently, we must accept the fact that nonequilibrium structures, local defects, grain boundaries, and in fact entire phases, are an important part of block copolymer phase behavior.[5–8] The low-energy defects are particularly important because they tend to survive the longest.

As usual, block copolymer studies typically begin with the simplest microstructure, the lamellar phase. Even this simple morphology exhibits a rich selection of grain boundaries,[5] of which the most common is undoubtedly the kink depicted in Fig. 1. Kink boundaries represent the only means of maintaining domain connectivity between large lamellar grains. Presumably, this results in a low grain boundary tension, which in turn is responsible for their relatively high population. This one-parameter family of boundaries is characterized by the angle θ between the lamellar normals of the two grains. Gido and Thomas[6] have surveyed the effect of θ on kink boundaries and have observed an interesting progression from smooth ''chevron'' kinks at low θ to elaborate ''omega'' kinks at high θ. In fact, they have speculated that these distinctive kink boundaries are separated by a phase transition at around $\theta \sim 90°$. More recent studies[9,10] have illustrated that kink boundaries play an important role in the behavior of the lamellar phase when it is subjected to shear. By applying large amplitude shear, Polis and Winey[9] have been able to produce an abundance of 90° kink boundaries that could provide the means of conducting more detailed experimental studies.

Some theoretical effort has already been directed towards kink boundaries. Gido and Thomas[6] have included along with their experimental study some theoretical predictions based on the strong-segregation theory (SST) of Semenov.[11] Although SST calculations do not accurately represent experiments,[12] which are typically performed at intermediate segregations, they are renowned for producing simple intuitive explanations for block copolymer behavior. However, due to the complexity of the kink boundary, Gido and Thomas found it necessary to supplemented the SST with several additional approximations, which we think compromise the validity of their conclusions. More recently, Netz *et al.*[13] examined kink boundaries using a phenomenological Landau-Ginzburg model. The virtue of this approach is its simplicity and generality. However, the relevance of their results to the intermediate-segregation regime is uncertain since their model is based on a weak-segregation expansion.

At present, the most reliable theory in the intermediate-segregation regime is the self-consistent field theory (SCFT) of Helfand.[14] The reason for its limited application to block copolymer systems has been the complexity involved in its implementation. However, this difficulty has been recently overcome for infinitely-periodic morphologies.[15] Here, we demonstrate how the technique can be extended to treat an interface between two separate periodic structures. The ap-

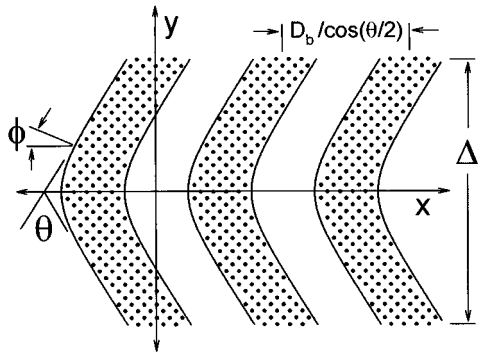

FIG. 1. Schematic illustration of the lamellar kink grain boundary. The middle of the boundary is positioned at $y=0$; by $y=\pm\Delta/2$, we assume the melt has relaxed to the bulk lamellar phase with a period D_b. The angle between the two lamellar orientations is specified by θ, and the local orientation of the A/B interface is specified by ϕ.

plication of this method requires the repeat period of the two structures to be identical in the plane of the interface; i.e., the phases must be epitaxially matched. However, this condition is satisfied in many situations including the kink boundaries discussed above. Therefore, lamellar kinks provide an appropriate interface on which to illustrate our method. Specifically, we examine kink boundaries in a monodisperse AB diblock copolymer melt as a function kink angle θ, the degree of segregation χN, the composition of the diblock f, and the conformational asymmetry a_A/a_B. Consistent with experiment,[6] we find a phase transition separating chevron- and omega-type kinks.

II. THEORY

Here, we apply the self-consistent field theory (SCFT) method in Ref. 15 to examine the grain boundary depicted in Fig. 1. As in Ref. 15, we consider a melt containing n AB diblock copolymers, where the A and B blocks consist of fN and $(1-f)N$ segments, respectively. The segments are assumed to be incompressible and are defined based on a common volume, $1/\rho_0$. Hence, the total volume of the melt is $\mathscr{V}=nN/\rho_0$. The SCFT used here assumes completely flexible Gaussian A and B segments with statistical lengths a_A and a_B, respectively, from which an average length is defined as $a\equiv[fa_A^2+(1-f)a_B^2]^{1/2}$; although Ref. 15 only considers $a_A=a_B$, the generalization to $a_A\neq a_B$ is straightforward.[16] The standard Flory-Huggins parameter, χ, is used to express the incompatibility between A and B segments.

The SCFT method in Ref. 15 is described for infinitely-periodic microstructures. However, it can be applied equally well to systems that are periodic in some directions and finite in the remaining directions.[17] To do so just requires an appropriate set of basis functions with which all spatially-dependent quantities can be expanded. For convenience, the basis functions should be orthonormal and eigenfunctions of the Laplacian operator. For the grain boundary depicted in Fig. 1, they must be invariant under the interchange $(x,y,z)\rightarrow(x,-y,z)$, because of the reflection symmetry about $y=0$. At the edges, $y=\pm\Delta/2$, each lamellae is locally symmetric with respect to a 180° rotation about an axis perpendicular to the plane of the figure passing through its center. This condition can be enforced by requiring the basis functions to be invariant under the mapping $(x,y,z)\rightarrow(-x,\Delta-y,z)$. Note that this latter constraint breaks the translational invariance in the x-direction by forcing the center of a lamellae to pass through $(0,\Delta/2,z)$, as illustrated in Fig. 1. The set of basis functions, which satisfy these symmetries, are

$$f_{mn}(\mathbf{r})=\begin{cases} C_mC_n\cos(mk_xx)\cos(nk_yy), & \text{if } n \text{ is even,}\\ C_mC_n\sin(mk_xx)\cos(nk_yy), & \text{if } n \text{ is odd,}\end{cases} \tag{1}$$

where $m,n=0,1,2,\ldots$, $k_x=2\pi\cos(\theta/2)/D_b$, $k_y=\pi/\Delta$, and D_b equals the bulk lamellar period. Clearly, $m=0$ is not permitted if n is odd. The coefficients C_i are determined by the orthonormal condition,

$$\frac{1}{\mathscr{V}}\int f_{mn}(\mathbf{r})f_{m'n'}(\mathbf{r})d\mathbf{r}=\delta_{mm'}\delta_{nn'}, \tag{2}$$

which requires $C_0=1$ and $C_i=\sqrt{2}$ for $i>0$. Because these functions form an infinite set, they must be truncated in order to perform a calculation. Generally, we include all functions with $m\leqslant m_{\max}$ and $n\leqslant n_{\max}$. Ideally Δ should also be infinite, but it is necessary to choose a finite value. Then $m_{\max}$, $n_{\max}$, and Δ are increased until an acceptable error tolerance is met. The tolerance is always chosen small enough that all results are accurate to within the resolution of our plots, i.e., the linewidths. For the conditions examined here, we find that $m_{\max}=13$ and $n_{\max}=30$ to be more than sufficient. For $\theta\geqslant 30°$, $\Delta/aN^{1/2}\sim 5$ is generally fine, but for smaller angles, we use $\Delta/aN^{1/2}=150°/\theta$.

To calculate the grain boundary tension Γ_K for a particular degree of segregation χN, composition f, conformational asymmetry a_A/a_B, and tilt angle θ, we must first evaluate the free energy F_b and the domain spacing D_b of the bulk lamellar phase using the method described in Ref. 15. The bulk domain spacing is required in order to determine the period of the grain boundary in the x-direction, $D_b/\cos(\theta/2)$ (see Fig. 1). Given that, the free energy F of the grain boundary can be calculated using the basis functions above, Eq. (1), in conjunction with the technique described in Ref. 15. Once F has been evaluated, Γ_K is obtained using the relation,

$$\frac{\Gamma_KN^{1/2}}{k_BT\rho_0a}=\left(\frac{\Gamma_K\mathscr{A}_K}{nk_BT}\right)\left(\frac{\Delta}{aN^{1/2}}\right)=\left(\frac{F-F_b}{nk_BT}\right)\left(\frac{\Delta}{aN^{1/2}}\right), \tag{3}$$

where $\mathscr{A}_K\equiv\mathscr{V}/\Delta$ is the area of the grain boundary. As a by-product of the SCFT calculation, the A-segment profile $\phi_A(\mathbf{r})$ is provided, which contains a wealth of useful information regarding the grain boundary. This function varies between 0 and 1 depending on the fraction of A segments at $\mathbf{r}$. Because we assume the melt is incompressible, the B-segment distribution is given by $\phi_B(\mathbf{r})=1-\phi_A(\mathbf{r})$.

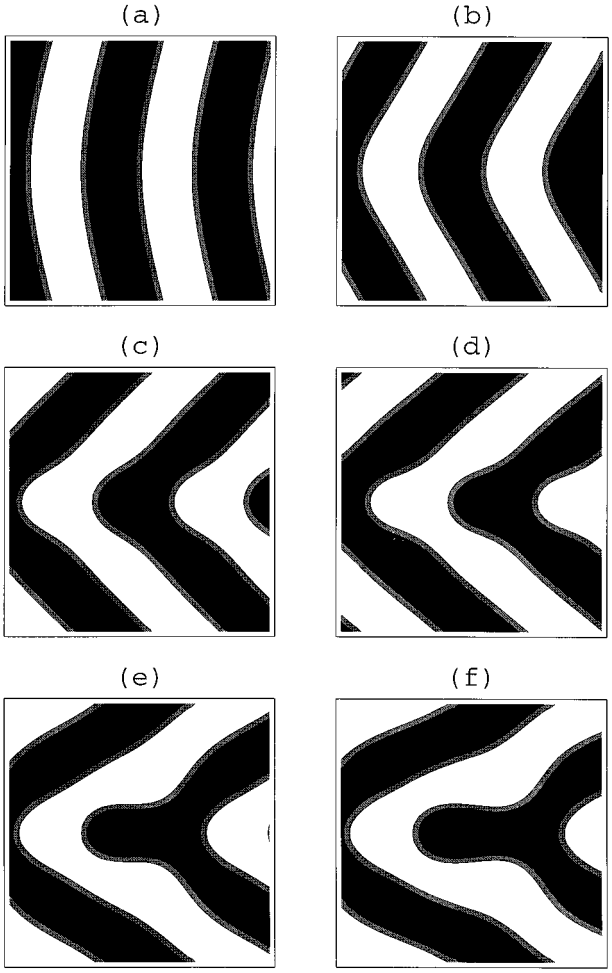

FIG. 2. Kink boundary profiles at angles (a) $\theta=30°$, (b) $\theta=60°$, (c) $\theta=90°$, (d) $\theta=100°$, (e) $\theta=110°$, and (f) $\theta=120°$ for a lamellar phase with $\chi N=20$, $f=0.5$, and $a_A=a_B$. The first two profiles, (a) and (b), are of chevron boundaries, the second two, (c) and (d), are intermediate boundaries, and the last two, (e) and (f), are omega boundaries. The A/B interfacial width is indicated by the gray region between contours for $\phi_A(\mathbf{r})=0.35$ and 0.65. The size of each image is 4×4 in units of $aN^{1/2}$, the RMS end-to-end length of an unperturbed diblock molecule.

III. EFFECTS DUE TO KINK ANGLE

We begin our study by examining how the grain boundary depicted in Fig. 1 varies with kink angle θ for symmetric diblocks (i.e., $f=0.5$ and $a_A=a_B$) at an intermediate degree of segregation $\chi N=20$. Figure 2 plots the segment profiles for $\theta=30°$, 60°, 90°, 100°, 110°, and 120°. These profiles are consistent with the experimental observations of Gido and Thomas.[6] The two low-angle kinks exhibit the ''chevron'' shape in which a smooth bend occurs in each of the lamellae. The two ''intermediate'' kinks in Figs. 2(c) and 2(d) exhibit small protrusions along the center of the grain boundary extending symmetrically from both the A and B domains. In the two high-angle kinks, the symmetry between the domains is broken producing the ''omega'' shape, where large protrusions occur but only in either the A or B domains.

The behavior of an ordered AB block copolymer melt is influenced by three considerations: the curvature of the internal A/B interface, the A/B interfacial tension, and packing frustration.[1] The local mean-curvature, H, of the A/B interface affects the relative stretching energy between the A and B blocks, and in order to balance their energies, the interface tends to select a particular spontaneous curvature, H_0, which is zero when the diblocks are symmetric. ($H\equiv(C_1+C_2)/2$, where C_1 and C_2 are the principal curvatures at a point on the A/B interface.[1]) Deviations from $H=H_0$ cause an increase in the free energy of the melt, which is approximately proportional to $E_H\equiv\int(H-H_0)^2d\mathscr{A}$ integrated over the A/B interface.[18] To monitor its effect on the boundary, we calculate the excess contribution, $E_{H,\mathrm{ex}}$, produced by the kink. The A/B interfacial tension, γ_{AB}, simply acts to minimize interfacial area. We examine its effect by evaluating the excess A/B interfacial area $\mathscr{A}_{\mathrm{AB,ex}}$ due to the grain boundary. ($\mathscr{A}_{\mathrm{AB,ex}}\equiv\mathscr{A}_{\mathrm{AB}}-2\mathscr{V}/D$, where $\mathscr{A}_{\mathrm{AB}}\equiv\int d\mathscr{A}$ is the total A/B interfacial area.) The third consideration in a block copolymer melt is packing frustration produced by variation in the domain thickness, which causes excessive stretching in some of the chains. To gauge the degree of packing frustration, we locate the point in the microstructure furthest from an A/B interface and define that distance as $d_{\max}$. (In a symmetric lamellar phase, $d_{\max}=D_b/4$, which is half the width of a lamella.) In order to explain the progression of the kink boundary with angle, we plot the above three quantities, $E_{H,\mathrm{ex}}$, $\mathscr{A}_{\mathrm{AB,ex}}$, and $d_{\max}$, as a function of θ in Fig. 3.

At low angles, the chevron shape in Figs. 2(a) and 2(b) is preferred because it only causes small deviations from the spontaneous curvature, it reduces the A/B interfacial area, and it produces very little packing frustration. Although, this shape causes an energy reduction due to the negative value of $\mathscr{A}_{\mathrm{AB,ex}}$, the energy penalties for $E_{H,\mathrm{ex}}>0$ and $d_{\max}>D_b/4$ prevent the grain boundary tension from becoming negative. In the chevron kink, packing frustration occurs at the center of the boundary where the layer thickness causes $d_{\max}$ to increase as $D_b/4\cos(\theta/2)$. This would eventually produce excessive degrees of packing frustration, and consequently, there comes a point, $\theta=78°$ in this case,[19] where the grain boundary must deviate from this trend. It does so by forming symmetric protrusions characteristic of the intermediate shape in Figs. 2(c) and 2(d). Although the intermediate boundary produces a significant increase in $\mathscr{A}_{\mathrm{AB,ex}}$, that is compensated for by the large reduction in $d_{\max}$. Evidently, the A/B interfacial bending energy (i.e., $E_{H,\mathrm{ex}}$) does not significantly influence this transformation. Note that our distinction between chevron and intermediate boundaries is a somewhat arbitrary criterion related to the A/B interfacial shape. It certainly does not imply a phase transition in the grain boundary.

Based on Fig. 3, it seems obvious that the omega shape in Figs. 2(e) and 2(f) results from a reduction in curvature energy [see Fig. 3(a)]. The cylindrical end caps on the large protrusions contribute significantly to $E_{H,\mathrm{ex}}$, and thus it is advantageous to reduce the number of protrusions by switching from an intermediate to an omega boundary. Evidently, this is enough to compensate for the increase in A/B interfacial area produced by the omega boundary [see Fig. 3(b)]. It

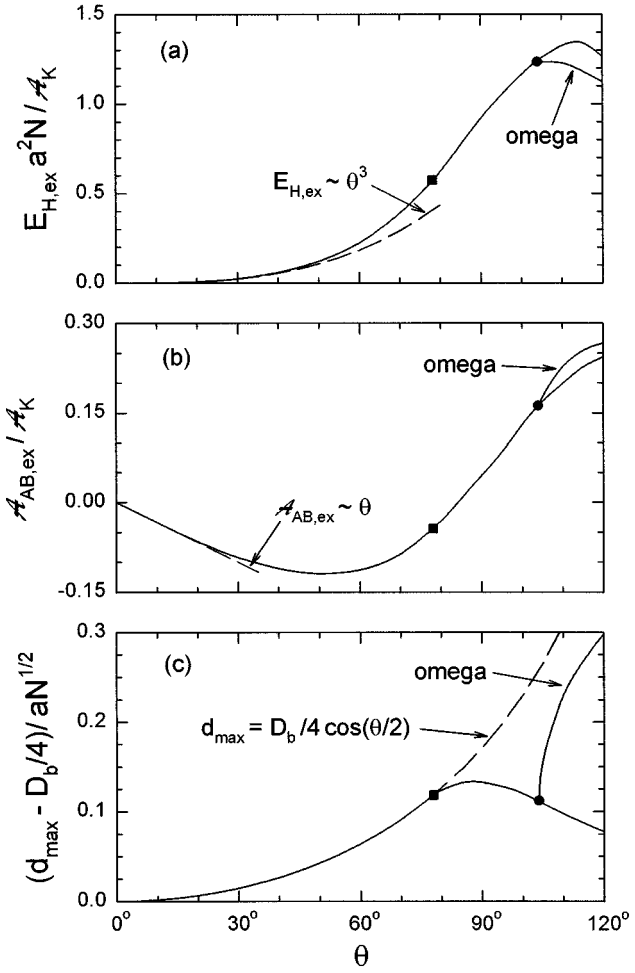

FIG. 3. Three factors important to the behavior of a block copolymer melt are examined as a function of kink angle. In (a), $E_{H,\mathrm{ex}}$ reflects the bending energy penalty due to the kink boundary. In (b), $\mathscr{A}_{\mathrm{AB,ex}}$ is the excess A/B interfacial area produced by the kink. In (c), $d_{\max}-D_b/4$ measures the increase in domain thickness compared to the bulk lamellar phase. These quantities are all calculated for $\chi N=20$, $f=0.5$, and $a_A=a_B$. The crossover from the chevron to the intermediate boundary indicated by the solid squares occurs when $d_{\max}$ departs from the dashed curve corresponding to $D_b/4\ \cos(\theta/2)$. The solid dots denote the phase transition from the intermediate boundary to the lower-energy omega boundary.

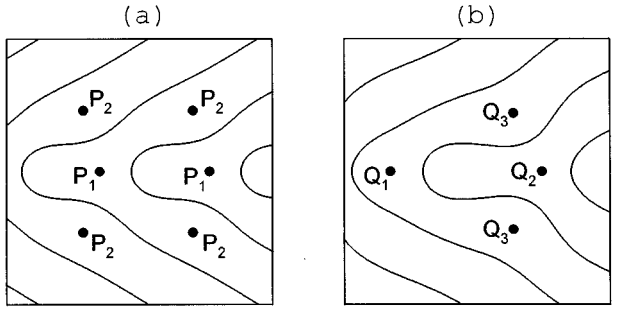

FIG. 4. A/B interfaces in the (a) intermediate and (b) omega kink boundaries calculated for $\theta=120°$, $\chi N=20$, $f=0.5$, and $a_A=a_B$. Locations within the microdomains responsible for high degrees of packing frustration are indicated by the solid dots. The size of each image is 4×4 in units of $aN^{1/2}$.

also appears that the reduction in $E_{H,\mathrm{ex}}$ compensates for a huge increase in packing frustration [see Fig. 3(c)]. However, this is not necessarily the case, because $d_{\max}$ is no longer a good indicator of frustration. At high kink angles, there are several distinct points in the boundary that contribute to the packing frustration. Figure 4 plots the domain shapes for the intermediate and omega boundaries at $\theta=120°$, and indicates those locations most responsible for the frustration. In Fig. 4(a), P_1 is the point that defines $d_{\max}$ and in Fig. 4(b) it is Q_1. Notice that Q_1 occurs only half as often as P_1. We should really compare the average effect of Q_1 and Q_2 to that of P_1, and on that basis, P_1 likely produces more frustration. Off the axis of the grain boundary, Q_3 may produce a bit more frustration than P_2, but its overall effect is no doubt less because it occurs half as often. Although it is virtually impossible to quantify the effects of frustration, these observations suggest the omega boundary lowers the overall packing frustration. Note that the intermediate and omega kinks represent distinct solutions in the SCFT, and therefore they are separated by a well-defined phase transition that will produce a singularity in the grain boundary tension. By closely examining the degree of asymmetry in the omega boundary, we conclude that this is a continuous transition as suggested earlier by Gido and Thomas.[6]

The grain boundary tension is plotted in Fig. 5 as a function of angle for a symmetric diblock melt at $\chi N=20$. In the small-angle regime, the tension obeys a $\Gamma_K\sim\theta^3$ scaling law indicated by the dashed line.[13,21] At $\theta=78°$, the intermediate boundary occurs and Γ_K begins to deviate significantly from the dashed line. Following that, the continuous symmetry-breaking transition occurs at $\theta=104°$ producing three mean-field kink boundary solutions: the intermediate boundary and two lower-energy omega boundaries. The omega solutions have equal energies and differ only in the interchange of A and B domains. In Fig. 5, we plot their tension as well as that of the intermediate boundary. The two omega solutions rep-

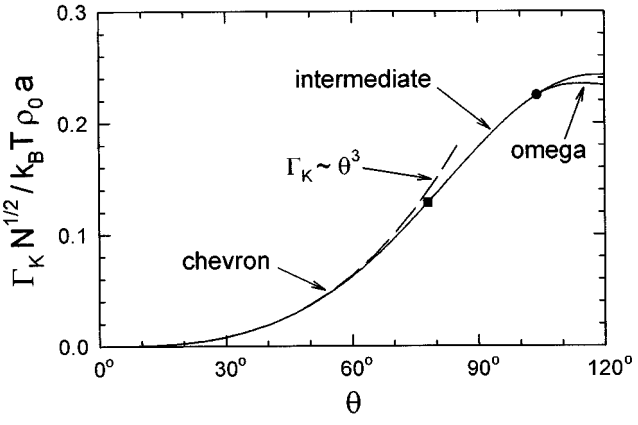

FIG. 5. Grain boundary tension as a function of angle for $\chi N=20$, $f=0.5$, and $a_A=a_B$. The dashed line corresponds to $\Gamma_K\sim\theta^3$. The solid square indicates the crossover from the chevron to the intermediate kink as defined in Fig. 3(c), and the solid dot indicates the phase transition to the omega kink. At angles above the phase transition, both the intermediate and omega grain boundary tensions are plotted.

resent local minima in the free energy surface, and the intermediate solution is a higher-energy saddle point located between them. The difference between the intermediate and omega surface tensions represents the barrier that must be overcome in order to traverse between the two omega solutions. Because the barrier is small (see Fig. 5), there is a reasonable probability that an omega kink will switch between A- and B-type protrusions along a single grain boundary. In fact, this has already been observed experimentally.[6]

At very high kink angles, the domains begin forming a series of steps extending outward from the grain boundary, consistent with experimental observation (see the boundary labeled E in Fig. 11 of Ref. 6). This rather complicated shape can require a particularly large number of basis functions (i.e., $m_{\max}n_{\max}\gg 400$) to accurately describe it, and this has prevented us from looking much beyond $\theta=120°$. Nevertheless, we have confirmed that Γ_K starts to decrease with angle, consistent with a previous prediction in Ref. 13. Furthermore, results not shown here suggest that a discontinuous transition occurs at $\theta\sim 130°$ beyond which protrusions again occur symmetrically in the A and B domains. Regardless, we speculate that the sharp bends created by the series of steps will facilitate the breakage and reformation of lamellae which in turn will destroy the metastability of the kink boundary. This would explain why kink boundaries are rarely observed[6] for $\theta>120°$ despite the reduction in Γ_K.

To appreciate how small the grain boundary tension is in Fig. 5, we compare it to the A/B interfacial tension, γ_{AB}. Based on strong-segregation theory (SST), the A/B tension is estimated by $\gamma_{\mathrm{AB}}N^{1/2}/k_BT\rho_0 a=(\chi N/6)^{1/2}$, which yields a value of 1.8 at $\chi N=20$. (This equation is for conformationally symmetric diblocks; the more general expression for $a_A\neq a_B$ is given in Ref. 20.) This is almost an entire order of magnitude greater than the maximum grain boundary tension calculated for a kink! We can also compare the kink boundary tension to that of a ''T-junction'' boundary,[6] where the lamellae in one grain are parallel to the boundary and the lamellae of the other grain are perpendicular. T-junctions occur far less often than kinks,[6] presumably because they possess a relatively high tension. Although there are no SCFT calculations for T-junctions, we can estimate their tension from free energy calculations for the mixed lamellar phases in thin film geometries.[17] Based on those calculations, we predict a T-junction tension of about 0.2 at $\chi N=20$, which is comparable to the maximum kink boundary tension; results in Ref. 13 lead to the same conclusion.

We have noticed several quantities, $E_{H,\mathrm{ex}}$, $\mathscr{A}_{\mathrm{AB,ex}}$, and Γ_K, that scale with θ at small angles. This behavior can be explained by making a small-angle approximation,

$$\frac{\Gamma_K N^{1/2}}{k_BT\rho_0 a}\approx\int_{-\infty}^{\infty}\left[\frac{K}{2}\left(\frac{d\phi}{dY}\right)^2+\frac{B}{8}\left(\frac{\theta^2}{4}-\phi^2\right)^2\right]dY, \tag{4}$$

where ϕ is defined in Fig. 1 and $Y\equiv y/aN^{1/2}$. This expression assumes that both ϕ and θ are small and that they are expressed in radians. It also assumes that the diblock molecule is symmetric. The first term represents the bending energy of an A/B interface; K is a dimensionless bending modulus and $H\approx(d\phi/dY)/2aN^{1/2}$. The second term is the penalty for deviations from the preferred lamellar thickness; B is a dimensionless compression modulus and the local increase in the lamellar period is approximately $D_b(\theta^2/4-\phi^2)/2$. In the next section, we provide SST expressions for these two moduli. Within SCFT, only the second one is straightforward to calculate [see Eq. (14) below]; for $\chi N=20$, we find that $B=4.17$. Minimizing Eq. (4) by standard methods,[21] we obtain the relation,

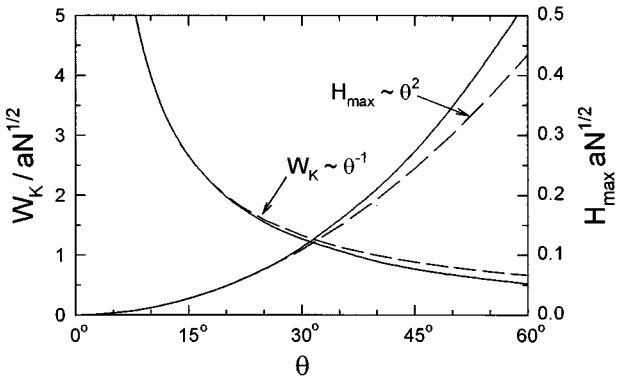

FIG. 6. Width of the grain boundary W_K and the A/B interfacial curvature $H_{\max}$ at the center of the grain boundary plotted as a function of the kink angle θ with $\chi N=20$, $f=0.5$, and $a_A=a_B$. The width W_K is defined as the interval where $-\theta/4<\phi<\theta/4$ (see Fig. 1). The dashed lines are fits to Eqs. (6) and (7) with $K/B=40.1$.

$$\phi=\frac{\theta}{2}\tanh\left[\frac{\theta}{4}\left(\frac{B}{K}\right)^{1/2}Y\right]. \tag{5}$$

From this it follows that the maximum curvature $H_{\max}$ at the center of the kink is

$$H_{\max}aN^{1/2}\approx\frac{1}{2}\left(\frac{d\phi}{dY}\right)_{Y=0}=\frac{1}{16}\left(\frac{B}{K}\right)^{1/2}\theta^2, \tag{6}$$

and that the width W_K of the kink boundary defined as the interval between $\phi=\pm\theta/4$ is

$$\frac{W_K}{aN^{1/2}}\approx 4\ln(3)\left(\frac{K}{B}\right)^{1/2}\theta^{-1}. \tag{7}$$

Fitting these two equations to the SCFT results in Fig. 6 provides a consistent ratio of the two moduli, $B/K=40.1$. Using $B=4.17$, it then follows that $K=0.104$, which is consistent with the value calculated in Ref. 22. Using these moduli, $dx/dy\approx\phi$, and Eq. (5), we can calculate the shape of a small-angle kink. Figure 7 confirms that the shape coincides with the $\theta\to 0$ limit of the SCFT. Now based on this small-angle approximation,

$$\frac{E_{H,\mathrm{ex}}a^2N}{\mathscr{A}_K}\approx\frac{aN^{1/2}}{2D_b}\int_{-\infty}^{\infty}\left(\frac{d\phi}{dY}\right)^2dY=\frac{aN^{1/2}}{24D_b}\left(\frac{B}{K}\right)^{1/2}\theta^3, \tag{8}$$

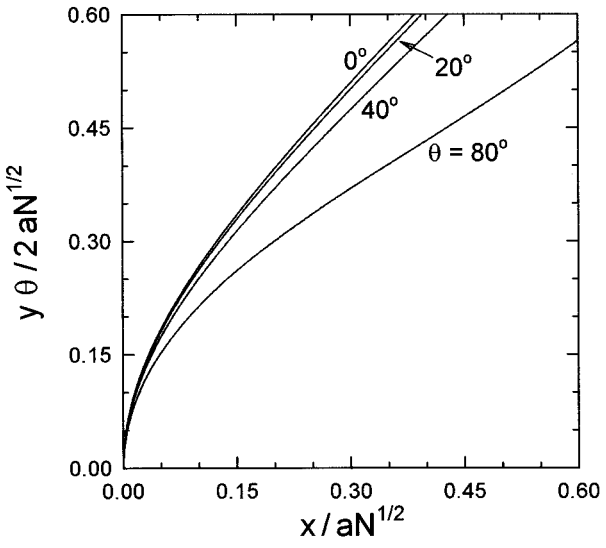

FIG. 7. Shapes of the A/B interface (defined by $\phi_A(\mathbf{r})=0.5$) calculated for symmetric diblocks at $\chi N=20$ over a range of kink angles. The $\theta=0°$ curve is obtained using Eq. (5) with $K/B=40.1$, and the other curves are calculated using the full SCFT. The y-axis is scaled by $\theta/2$ expressed in radians. Only the $y>0$ half of the interface is shown and the curves are shifted in the x-direction so that they each pass through the origin.

$$\frac{\mathscr{A}_{\mathrm{AB,ex}}}{\mathscr{A}_K}\approx-\frac{aN^{1/2}}{D_b}\int_{-\infty}^{\infty}\left(\frac{\theta^2}{4}-\phi^2\right)dY=-\frac{2aN^{1/2}}{D_b}\left(\frac{K}{B}\right)^{1/2}\theta, \tag{9}$$

$$\frac{\Gamma_K N^{1/2}}{k_BT\rho_0 a}\approx\frac{1}{12}(KB)^{1/2}\theta^3. \tag{10}$$

In Figs. 3(a), 3(b), and 5 the dashed lines represent these three approximations evaluated with the above values of K and B; the agreement with the full SCFT calculation is excellent.

IV. EFFECTS DUE TO SEGREGATION

Next, we examine the effects of segregation on the grain boundary. Figure 8 shows profiles at $\chi N=11$, 15, 20, and 30 for a $\theta=90°$ kink boundary formed by a symmetric diblock. The profile at $\chi N=11$ is weakly segregated, while the other three represent intermediately segregated cases. The weakly segregated profile is rather distinctive; the lamellae exhibit a periodic modulation extending outward from the grain boundary. The amplitude and the distance over which these modulations extend increases as the segregation is reduced. At some point, this causes the lamellae to break up into cylinders destroying the kink boundary and preventing us from extending our results to the order-disorder transition (ODT) at $\chi N=10.495$. Reference 13 also observes these modulations, but does not report similar problems near the ODT. Regardless, this behavior would be severely modified by fluctuation effects omitted by our SCFT treatment, but fortunately these effects are limited to small degrees of segregation.[26] Above $\chi N\sim 12$, the profiles become well developed, the modulations disappear, and we expect the SCFT to produce experimentally accurate results. As illustrated in

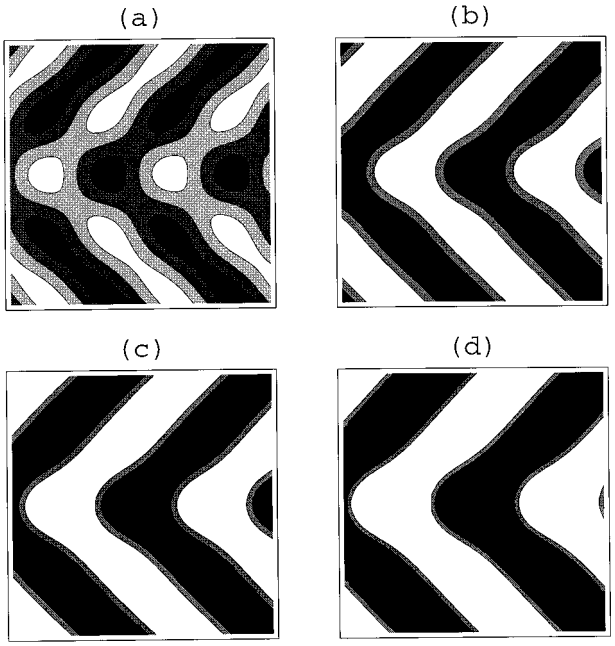

FIG. 8. $\theta=90°$ kink boundaries in a symmetric lamellar phase at (a) $\chi N=11$, (b) $\chi N=15$, (c) $\chi N=20$, and (d) $\chi N=30$. In each plot, contours are shown for $\phi_A(\mathbf{r})=0.35$ and 0.65; because of the large A/B interfacial width in (a), an additional contour at 0.5 is included. The size of each image is 4×4 in units of $aN^{1/2}$.

Fig. 9, a well-defined shape for the grain boundary quickly emerges as the degree of segregation is increased. In fact, the domains for $\chi N=20$ and 30 are so similar when scaled by their respective lamellar periods, that they cannot be distin-

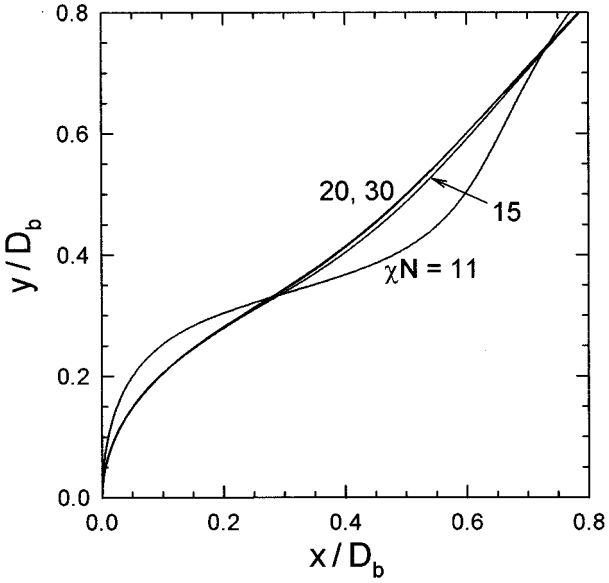

FIG. 9. Shape of the A/B interface (defined by $\phi_A(\mathbf{r})=0.5$) in $\theta=90°$ kink boundaries formed by symmetric diblocks. The curves for $\chi N=11$, 15, 20, and 30 are all scaled by their lamellar period, $D_b/aN^{1/2}=1.348$, 1.516, 1.651, and 1.828, respectively. The curves for $\chi N=20$ and 30 are indistinguishable on this scale. Only the $y>0$ half of the interface is shown and the curves are shifted in the x-direction so that they each pass through the origin.

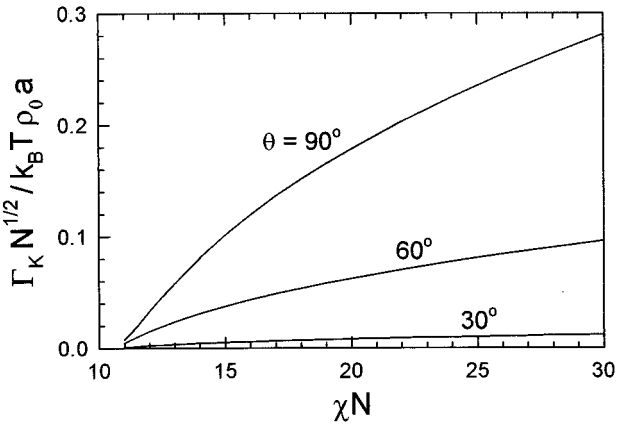

FIG. 10. Grain boundary tension as a function of segregation for $\theta=30°$, 60°, and 90°. Calculations are all performed for symmetric diblock molecules, i.e., $f=0.5$ and $a_A=a_B$.

guished from each other in Fig. 9. As indicated in Fig. 8, the main effects of increasing χN are a magnification in domain size due to chain stretching and a reduction in A/B interfacial width due to localization of the diblock junctions. Notice that the A/B interfacial width remains extremely uniform throughout the kink boundary with the exception of Fig. 8(a).

Figure 10 shows the grain boundary tension calculated as a function of segregation for symmetric diblocks at angles of $\theta=30°$, 60°, and 90°. Even at $\chi N=30$, the melt conditions are far from the strong-segregation limit; although the domains are relatively pure, the chains are only weakly stretched.[12] Nevertheless, it is still useful to consider how our results would extend to the $\chi N=\infty$ limit. We know that at strong segregations, the kink boundary approaches an asymptotic shape and its linear size scales as $\chi^{1/6}N^{2/3}$.[1,11] The excess free energy per chain increases as $\chi^{1/3}N^{1/3}$,[1,11] and so the excess energy per unit volume scales as $\chi^{1/3}N^{-2/3}$. Since the width of the grain boundary increases as $\chi^{1/6}N^{2/3}$, the excess energy per unit area, i.e., the grain boundary tension, scales as $\Gamma_K\sim\chi^{1/2}$, which is the same scaling exhibited by the A/B interfacial tension.[20] These arguments are general to all grain boundaries in the strong-segregation limit. Fitting our SCFT results at $\chi N=30$ for the three angles in Fig. 3 produces exponents of about 0.9, which is significantly larger than the SST prediction of 0.5. This is not surprising, since strong-segregation scaling typically requires far higher degrees of segregation.[2]

We can also evaluate the small-angle approximation from the previous section using SST. In this limit, the free energy F_b of a symmetric diblock lamellar phase with a period D and a slight curvature H is[11,18,23]

$$\frac{F_b}{nk_BT}=\frac{\pi^2}{32}\left(1+\frac{3}{16}H^2D^2\right)\left(\frac{D}{aN^{1/2}}\right)^2+2\left(\frac{\chi N}{6}\right)^{1/2}\left(\frac{D}{aN^{1/2}}\right)^{-1}. \tag{11}$$

Minimizing F_b tells us that the preferred curvature is $H=0$ and the preferred domain spacing is given by

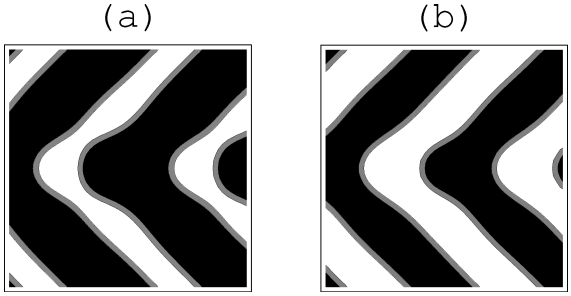

FIG. 11. Profiles of $\theta=90°$ kink boundaries produced by asymmetric diblocks at $\chi N=20$. In (a) $f=0.34$ and $a_A/a_B=1.0$, and in (b) $f=0.5$ and $a_A/a_B=2.0$. To indicate the width of the A/B interface, contours are plotted at $\phi_A(\mathbf{r})=0.35$ and 0.65. The size of each image is 4×4 in units of $aN^{1/2}$.

$$\frac{D_b}{aN^{1/2}}=2\left(\frac{8\chi N}{3\pi^4}\right)^{1/6}. \tag{12}$$

Using Eq. (11), we can evaluate the two moduli in Eq. (4) by taking the appropriate derivatives of F_b about its minimum,

$$K\equiv\frac{1}{4a^2N}\left(\frac{\partial^2}{\partial H^2}\frac{F_b}{nk_BT}\right)_{H=0,D=D_b}=\frac{3}{16}\left(\frac{\chi N}{3\pi}\right)^{2/3}, \tag{13}$$

$$B\equiv D_b^2\left(\frac{\partial^2}{\partial D^2}\frac{F_b}{nk_BT}\right)_{H=0,D=D_b}=\frac{3\pi}{2}\left(\frac{\chi N}{3\pi}\right)^{1/3}. \tag{14}$$

Inserting these expression into Eqs. (7) and (10), we confirm that $W_K\sim\chi^{1/6}N^{2/3}$ and $\Gamma_K\sim\chi^{1/2}$, respectively. We also notice that these strong-segregation expressions are rather inaccurate at the degrees of segregation considered here. For $\chi N=20$, the SST expressions give $B=6.06$ and $K=0.310$ as compared to $B=4.17$ and $K=0.104$ using SCFT.

V. EFFECTS DUE TO MOLECULAR ASYMMETRY

Up to this point, our attention has been restricted to symmetric diblocks (i.e., $f=0.5$ and $a_A=a_B$). We now explore the effect of introducing an asymmetry to the $\theta=90°$ kink boundary in Figs. 2(c) and 8(c). Figure 11(a) shows the result of reducing the composition to $f=0.34$, which is next to the lamellar/gyroid transition.[2] With this asymmetry, the minority domain (shown in white) begins to pinch off. A further reduction in f will presumably break the connectivity of the minority domains leaving their lamellae with cylindrical end caps and producing an array of cylinders along the center of the grain boundary. The cylindrical A/B interfaces become energetically favorable due to the spontaneous curvature H_0 produced by the molecular asymmetry. Figure 12(a) shows that the compositional asymmetry leads to a reduction in the grain boundary tension, and that the reduction is most significant for the high-energy kinks.

Conformational asymmetry is typically ignored in block copolymer calculations and so our understanding of its effect is somewhat less than that of compositional asymmetry. Figure 11(b) shows the 90° kink for an asymmetry of $a_A/a_B=2.0$. Because f is still 0.5, both domains remain equal in size. Instead of changing the relative domain volumes, this asymmetry makes the A domains (shown in white) easier to

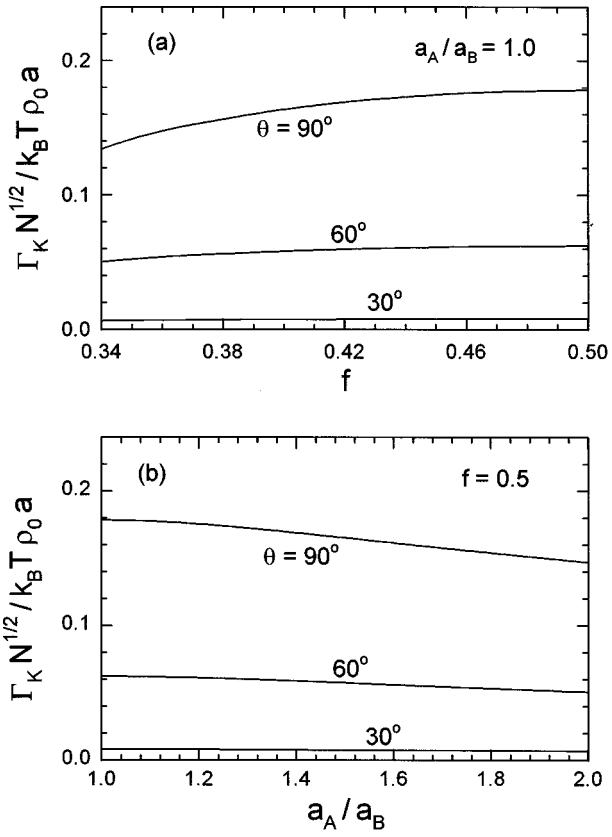

FIG. 12. Grain boundary tensions for $\theta = 30°$, 60°, and 90° kinks formed by asymmetric diblocks at $\chi N = 20$. In (a), the composition of the diblock is varied with $a_A = a_B$, and in (b), the conformational asymmetry is varied with $f = 0.5$.

deform, because segments with longer statistical lengths are easier to stretch. Consequently, the influence of packing frustration is reduced in the A domains, and in accord with our discussion above, they exhibit less of a protrusion. Figure 12(b) illustrates that again the block copolymer asymmetry reduces the grain boundary tension, assuming that we compare melts with the same average segment length (i.e., equal a). As before, the effect of the molecular asymmetry is greatest for the high-energy boundaries.

The scaling behavior discussed above for symmetric diblocks also applies to asymmetric ones. Referring to Ref. 16, it is clear that our arguments for the strong-segregation scaling, $\Gamma_K \sim \chi^{1/2}$, still hold. It is less clear that the $\Gamma_K \sim \theta^3$ scaling will remain given that the asymmetry causes a finite spontaneous curvature H_0 in the A/B interfaces,[18] which produces a linear term in the bending energy of Eq. (4). However, adjacent interfaces have spontaneous curvatures in the opposite directions causing the linear contribution to vanish. Consequently, the energy density in the kink continues to scale as curvature squared, and the grain boundary tension continues to obey $\Gamma_K \sim \theta^3$ at small angles. We have confirmed this for both types of asymmetry using the full SCFT calculation.

VI. DISCUSSION

There have been few theoretical attempts to address the grain boundaries in block copolymer melts. Gido *et al.*[6,7] have put forth several arguments based on strong-segregation theory (SST) to explain some of their experimental observations. However, these calculations had to assume an A/B interfacial shape, which was guided by their belief in an overwhelming tendency to form constant mean curvature (CMC) interfaces.[5] Since then, it has been illustrated that large deviations from CMC are common,[2] and in fact kink boundaries represent another situation where this happens. Perhaps more dangerous was their assumption that the polymer chains follow straight paths normal to the interface. While these conditions tend to be satisfied in the classical block copolymer morphologies, they by no means represent constraints on the polymer chains. Thus their arguments, explaining for example the occurrence of the omega shape in large-angle kinks, are not fully justified. With new strong-segregation methods developed by Likhtman and Semenov,[24] which account for curved polymer paths and allow surfaces to acquire an equilibrium shape, better SST calculations are now possible.

More recently, Netz *et al.*[13] have examined boundaries between periodic phases using a phenomenological Landau-Ginzburg model. Their Hamiltonian has one term that drives phase separation, gradient terms to select a preferred domain size, and entropy of mixing terms. Since A and B blocks are joined to form a single molecule, there is no entropy of mixing in the diblock system; the entropy terms should just be considered as a convenient way of keeping the order parameter in the desired range. Since their phenomenological model contains the same ingredients as our simple Hamiltonian in Eq. (4), it naturally exhibits similar behavior at small kink angles. In fact, their grain boundary tension closely resembles ours (see Fig. 4) over the whole range of angles. Not surprisingly, the Landau-Ginzburg model also produces similar behavior to the SCFT at weak segregations. For instance, they observe modulations in the lamellae [see Fig. 8(a)], which in our case destroys the kink boundary just prior to the ODT. At strong segregations, the Landau-Ginzburg model breaks down and their grain boundary tension begins to decrease with increasing segregation. Furthermore, their model produces macrophase separation, which illustrates that the connection between A and B blocks is not strictly enforced. This is significant because it implies that packing frustration is not properly accounted for. Although they observe symmetric protrusions characteristic of our intermediate boundaries, they do not report any omega boundaries. We suspect that modeling omega kinks requires an accurate treatment of frustration. Reference 13 does not discuss the effect of molecular asymmetry on the kink boundary. To describe asymmetric diblocks, their Hamiltonian should include additional terms.[25] Furthermore, it would be necessary to know the relationship between the Landau-Ginzburg coefficients and the parameters of the diblock molecule in order to determine conformational asymmetry effects.

An advantage of the present approach is that it is based on a simple but realistic microscopic model and makes relatively few approximations; hence, it can produce quantitatively accurate predictions. Of course, some quantities such

as Γ_K would be difficult to measure directly, but they might be accessed indirectly through their effects on various behaviors. Other quantities, such as domain shapes and segment distributions could be compared directly with experiment. In particular, the angles corresponding to the evolution from chevron to omega kinks (i.e., $\theta=78°$ to 104°) are in good agreement with experiment.[6] Another strength of our more detailed approach is that spurious results, such as the decrease in Γ_K predicted in Ref. 13 at strong segregations, are less likely to occur because the model makes relatively few assumptions. The principle source of unphysical behavior in our SCFT approach results from the omission of fluctuation effects. However, these effects should only be important at weak segregations (i.e., $\chi N \lesssim 12$),[26] and therefore can be avoided. A further advantage of our SCFT approach is the ease with which it can be refined. For example, finite compressibility,[27] more general molecular interactions,[14,27] chain stiffness,[28] polydispersity, variations in architecture,[29] and added homopolymer[30] can all be accounted for.

VII. SUMMARY

In this paper, we have demonstrated the versatility of the SCFT for studying the boundaries between periodic block copolymer microstructures. This is illustrated by our study of kink grain boundaries in the AB diblock lamellar morphology. We begin by examining effects due to the kink angle. As a function of angle, the tension in a kink grain boundary increases from zero, peaks around $\theta\sim 120°$ and then decreases presumably to zero as θ approaches 180°.[13] In the small-angle regime, the tension scales as the cube of the angle.[13,21] Although the tension is lowest near $\theta=0°$ and 180°, kinks are not experimentally observed close to these limits.[6] We suggest that they are not identified at extremely low angles because the width of the grain boundary diverges as $W_K\sim\theta^{-1}$.[21] At very high angles, the lamellae start to exhibit a series of steps extending outward from the boundary, which are separated by sharp bends.[6] We suspect that these bends produce breaks in the lamellae which destroy the metastability of the boundary. Next, we address the effects of segregation. Because SCFT omits fluctuation effects, it cannot be trusted near the order-disorder transition. Nevertheless, χN only needs to exceed about 12 before SCFT begins to produce reasonable behavior. As χN reaches values of about 15, the shape of the kink boundary becomes well defined and further increases in segregation produce rather trivial effects: the domains increase in size due to chain stretching and the A/B interfacial width decreases due to localization of the diblock junctions. Naturally, increasing segregation also causes a monotonic increase in the grain boundary tension, which should eventually scale as $\Gamma_K\sim\chi^{1/2}$. Lastly, we examine the effect of molecular asymmetry. As either f deviates from 0.5 or a_A/a_B deviates from 1.0, a reduction in the grain boundary occurs. Although the decrease is very slight for small-angle kinks, it becomes significant as θ approaches 90°.

Our SCFT results for symmetric diblocks at $\chi N=20$ demonstrate an interesting evolution in domain shape as the kink angle θ is increased, which is consistent with the experimental observations of Gido and Thomas.[6] At low angles, the lamellae exhibit smooth kinks resembling a ''chevron'' shape. As θ exceeds 78°, small protrusions develop at the center of the boundary symmetrically in each of the A and B domains. This ''intermediate'' shape proceeds a continuous symmetry-breaking transition at $\theta=104°$ to an ''omega'' shape, where protrusions only occur in either the A or B domains. These transformations in domain shape can be explained in terms of the A/B interfacial bending energy, the A/B interfacial tension, and packing frustration.[1] At small angles, the smooth chevron shape is favored because it only produces small degrees of interfacial curvature, it lowers the interfacial area, and it maintains uniformly thick domains. However, at large angles, it produces excessive packing frustration at the center of the grain boundary. To relieve this, the intermediate shape occurs despite the significant rise it produces in the A/B interfacial area. Following that the omega shape occurs because reducing the number of protrusions results in less interfacial curvature and lowers the packing frustration further. It would be interesting to examine, either experimentally or theoretically, the effect of added homopolymer on the grain boundary. Such studies would shed more light on the role of packing frustration in the formation of the omega boundary. If our speculations are indeed correct, homopolymer should accumulate at the points indicated in Fig. 4(b), and furthermore could cause the omega boundary to convert back to a chevron shape. Needless to say, there are numerous other grain boundaries that could now be studied by SCFT, which would no doubt possess their own intriguing behavior.

ACKNOWLEDGMENTS

We are grateful to D. C. Morse for pointing out Ref. 21 and to M. Schick for supplying us with a copy of Ref. 13 prior to publication. We also appreciated their useful comments. F. S. Bates and others in the Department of Chemical Engineering at the University of Minnesota are acknowledged for their hospitality while this manuscript was being prepared.

[1] M. W. Matsen and F. S. Bates, Macromolecules **29**, 7641 (1996); J. Chem. Phys. **106**, 2436 (1997).
[2] M. W. Matsen and F. S. Bates, Macromolecules **29**, 1091 (1996).
[3] G. H. Fredrickson and F. S. Bates, Annu. Rev. Mater. Sci. **26**, 501 (1996); S. Qi and Z.-G. Wang, Phys. Rev. Lett. **76**, 1679 (1996); Phys. Rev. E **55**, 1682 (1997); J. G. E. M. Fraaije, B. A. C. van Vlimmeren, N. M. Maurits, M. Postma, O. A. Evers, C. Hoffmann, P. Altevogt, and G. Goldbeck-Wood, J. Chem. Phys. **106**, 4260 (1997).
[4] P. Lipic, J. Zhao, M. W. Matsen, D. A. Hajduk, M. B. Kossuth, and F. S. Bates (in preparation).
[5] B. L. Caralho, R. L. Lescanec, and E. L. Thomas, Macromol. Symp. **98**, 1131 (1995).
[6] S. P. Gido and E. L. Thomas, Macromolecules **27**, 6137 (1994).
[7] S. P. Gido, J. Gunther, E. L. Thomas, and D. Hoffman, Macromolecules **26**, 4506 (1993); S. P. Gido and E. L. Thomas, *ibid*. **27**, 849 (1994); **30**, 3739 (1997).
[8] D. A. Hajduk, H. Takenouchi, M. A. Hillmyer, F. S. Bates, M. E. Vigild, and K. Almdal, Macromolecules **30**, 3788 (1997).
[9] D. L. Polis and K. I. Winey, Macromolecules **29**, 8180 (1996).

[10] H. Wang, P. K. Kesani, N. P. Balsara, and B. Hammouda, Macromolecules **30**, 982 (1997).
[11] A. N. Semenov, Sov. Phys. JETP **61**, 733 (1985).
[12] M. W. Matsen and F. S. Bates, Macromolecules **28**, 8884 (1995).
[13] R. R. Netz, D. Andelman, and M. Schick, Phys. Rev. Lett. **79**, 1058 (1997).
[14] E. Helfand, J. Chem. Phys. **62**, 999 (1975); Macromolecules **8**, 552 (1975).
[15] M. W. Matsen and M. Schick, Phys. Rev. Lett. **72**, 2660 (1994).
[16] M. W. Matsen and F. S. Bates, J. Polym. Sci. Part B **35**, 945 (1997).
[17] M. W. Matsen, J. Chem. Phys. **106**, 7781 (1997).
[18] S. T. Milner and T. A. Witten, J. Phys. (France) **49**, 1951 (1988); Z.-G. Wang and S. A. Safran, *ibid*. **51**, 185 (1990); J. Chem. Phys. **94**, 679 (1991).
[19] The departure from $d_{\max}=D_b/4\cos(\theta/2)$ occurs when the A/B interfacial curvature at the center of the boundary plotted in Fig. 6 satisfies $H_{\max}=1/2d_{\max}$.
[20] E. Helfand and Z. R. Wasserman, Macromolecules **9**, 879 (1976).
[21] P. G. de Gennes and J. Prost, *The Physics of Liquid Crystals*, 2nd ed. (Clarendon, Oxford, 1993), p. 484.
[22] C. Yeung, A.-C. Shi, J. Noolandi, and R. D. Desai, Macromol. Theory Simul. **5**, 291 (1996).
[23] Z.-G. Wang, J. Chem. Phys. **100**, 2298 (1994).
[24] A. E. Likhtman and A. N. Semenov, Macromolecules (submitted).
[25] L. Leibler, Macromolecules **13**, 1602 (1980).
[26] S. A. Brazovskii, Sov. Phys. JETP **41**, 85 (1975); G. H. Fredrickson and E. Helfand, J. Chem. Phys. **87**, 697 (1987); V. E. Podneks and I. W. Hamley, JETP Lett. **64**, 617 (1996); I. W. Hamley and V. E. Podneks, Macromolecules **30**, 3701 (1997)
[27] E. Helfand and Y. Tagami, Polym. Lett. **9**, 741 (1971); J. Chem. Phys. **56**, 3592 (1971); **57**, 1812 (1972); E. Helfand and A. M. Sapse, *ibid*. **62**, 1327 (1975).
[28] M. W. Matsen, J. Chem. Phys. **104**, 7758 (1996).
[29] M. W. Matsen and M. Schick, Macromolecules **27**, 6761, 7157 (1994).
[30] M. W. Matsen, Phys. Rev. Lett. **74**, 4225 (1995); Macromolecules **28**, 5765 (1995).